

Article

A Multi-Parameter Flexible Smart Water Gauge for the Accurate Monitoring of Urban Water Levels and Flow Rates

Selamu Wolde Sebicho ^{1,*}, Baodong Lou ² and Bethel Selamu Anito ³¹ College of Mechanical and Electrical Engineering, Hohai University, Changzhou 213251, China² Institute of Intelligent Perception Innovation, Hohai University, Nanjing 211100, China; loubd@126.com³ College of Computer and Information Technology Engineering, Hohai University, Nanjing 211100, China; betselamanito@gmail.com

* Correspondence: selamujoky12@gmail.com

Abstract: Urban drainage and waterlogging prevention are critical components of urban water management systems, as they help to mitigate the risks of flooding and water damage in cities. The accurate collection of liquid level and flow rate data at the end of these systems is crucial for their effective monitoring and management. However, existing water equipment for this purpose has several shortcomings, including limited accuracy, inflexibility, and difficulty in operation under specific working conditions. A new type of multi-parameter flexible smart water gauge was developed to address these issues. This technology uses underwater simulation robot technology and is designed to overcome the deficiencies of existing water equipment. The flexibility of the gauge allows it to be adapted to different working conditions, ensuring accurate data collection even in challenging environments. The accuracy of the new water gauge was tested through a series of experiments, and the results showed that it was highly accurate in measuring both liquid level and flow rate. This new technology has the potential to be a key tool in smart water conservancy, enabling the more efficient and accurate monitoring of water levels and flow rates. By providing a new solution to the problem of collecting terminal equipment for urban drainage and waterlogging prevention, this technology can help to improve the resilience and sustainability of urban water management systems.

Keywords: smart water gauge; standard flow meter; water level; manhole cover; waterlogging prevention



Citation: Sebicho, S.W.; Lou, B.; Anito, B.S. A Multi-Parameter Flexible Smart Water Gauge for the Accurate Monitoring of Urban Water Levels and Flow Rates. *Eng* **2024**, *5*, 198–216. <https://doi.org/10.3390/eng5010011>

Academic Editor: Angeles Blanco

Received: 16 November 2023

Revised: 31 December 2023

Accepted: 12 January 2024

Published: 19 January 2024



Copyright: © 2024 by the authors. Licensee MDPI, Basel, Switzerland. This article is an open access article distributed under the terms and conditions of the Creative Commons Attribution (CC BY) license (<https://creativecommons.org/licenses/by/4.0/>).

1. Introduction

Monitoring water levels is crucial for managing water resources and ensuring environmental safety [1]. It is a vital component in understanding water regimes and is necessary for flood control and prediction [2,3]. Accurately measuring water levels is particularly important in monitoring, preventing, and mitigating the effects of natural disasters, such as floods. In urban areas, where floods can cause significant damage and losses, monitoring water levels is critical for reducing risk and preventing harm. Therefore, it is essential to conduct efficient and safe research on water level monitoring to reduce the economic and safety hazards associated with floods [4–7].

Urban drainage and waterlogging prevention have become one of the most concerning issues for urban residents due to the wide range of disasters that the flooding of urban settlements can lead to, causing both heavy property losses and casualties [8–11]. In addition, overflow pollution and other problems caused by urban drainage and waterlogging are becoming more and more serious, which directly leads to reductions in the operating efficiency of sewage treatment plants, seriously affects the safety of urban water supplies, and has become a major problem affecting social stability and restricting the sustainable development of the urban economy [12,13]. Therefore, it is urgent that we improve the

risk management ability of urban drainage and waterlogging prevention, reduce the problem of urban drainage and waterlogging disasters, and ensure the water safety of urban residents [14–16].

On the other hand, long-term pipeline leaks in urban drainage systems present a pressing concern in modern urban infrastructure management. These leaks, often undetected for extended periods, can result in adverse environmental impacts, compromised public health, and substantial economic costs. Urban drainage networks play a vital role in managing stormwater and wastewater flow, making the identification and mitigation of long-term leaks crucial for maintaining the functionality of these systems. Long-term pipeline leaks cause the soil to loosen and deposit nearby, leading to subsidence and landslides [17,18]. After a drainage pipeline ruptures, a seepage field is formed around the pipeline. Under the coupling effect of the seepage field and the surrounding soil, the mechanical properties of the soil change, forming a “groundwater pocket” mixed with soil and water [19]. This eventually leads to ground collapse accidents, which not only increase production costs but may also lead to casualties [20,21]. Therefore, it is essential that we conduct in-depth research on drainage pipe leakages and take corresponding measures to prevent the occurrence of accidents.

With the rise of smart cities, the status of more and more urban elements can be sensed in real time, and above-ground equipment, such as street lights, manhole covers, fire hydrants, video surveillance, and elevators, are connected to various system platforms through the Internet of Things [22,23]. Construction site dust diffusion monitoring, street noise monitoring, and other aerial data can be perceived and collected, thus solving many complex and uncertain problems in urban planning and improving the modernization level of urban governance capabilities. In contrast, urban drainage and waterlogging prevention face numerous concealed risks due to the inherent challenges of managing underground spaces. The lack of established management practices and comprehensive network management facilities for subterranean environments further exacerbates these risks when compared to surface-level city management. Additionally, the development of both urban drainage management systems and supportive sensors has lagged behind, hindering effective monitoring and mitigation efforts.

At present, the most commonly used water measuring instruments in China include the following: ultrasonic flowmeters (Doppler ultrasonic flowmeters), radar flowmeters (including non-contact water level, flow velocity, and flow measurement flowmeters), propeller flowmeters, bubble water level gauges, and pressure water level gauges. These existing sensors cannot detect the loosening and displacement of the soil under a pipeline very effectively. The gyroscope inside a flexible smart water gauge can monitor the attitude angle of the water gauge. The water gauge can be installed in the soil near the pipeline to detect the displacement of the soil, facilitating the timely identification of changes in soil layers near the pipeline.

In sewage pipeline and river detection, ultrasonic flowmeters rely on the reflection of bubbles and impurities in the water to measure the flow rate of the water; these meters occupy a significant amount of space and are susceptible to probe coverage by impurities, leading to failures [24,25]. Especially in sewage with high impurity contents, irregular alarms may occur. Radar flowmeters operate on the principle of the Doppler effect, generating electromagnetic waves on the water’s surface. When these waves encounter the moving water surface, they scatter and form an echo. By analyzing the frequency shift between the transmitted and received signals, the water surface velocity can be determined. These flowmeters are suitable for partially filled pipelines but are not applicable when the pipeline is full and the water reaches the top of the shaft.

Propeller flowmeters operate by the rotational motion of a paddle when flowing water acts on the sensing element [26,27]. The faster the water flows, the faster the paddle rotates, establishing a functional relationship between speed and flow rate, i.e., $V = F(n)$. However, these flowmeters only allow manual single measurements and cannot be monitored online

over an extended period. They are also unsuitable for locations with abundant aquatic plants and debris as they are prone to equipment damage.

Bubble water level gauges are unsuitable for well water level measurements [28,29]. Air bubbles in the wellbore may not accurately reach the wellhead, and the normal operation of these gauges is significantly affected by floating objects. Therefore, these gauges are not suitable for early warning systems in small and medium-sized rivers. In a sewage environment, pressure water level gauges may be obstructed by sediment burial, affecting their normal operation. Their unstable zero drift necessitates regular maintenance and calibration, making them unsuitable for measuring water levels in sewage wells.

Due to such technical limitations in existing water measuring equipment, a flexible smart water gauge was designed by our lab at Hohai University in 2021 for urban drainage and flood control. This paper introduces the principle of our flexible smart water gauge and presents our experimental results.

2. Flexible Smart Water Gauge

The subsequent sections focus on the flexible smart water gauge's basic principles, specifically focusing on the principles governing flow rate data acquisition. This section discusses the manhole cover terminal equipment flow rate calibration process, employing a standard flow meter for accuracy. Moving forward, Section 3 contains the results section, featuring the water level accuracy experiment, an experiment to verify the flexible smart water gauge's flow rate, and the implementation of an intelligent manhole cover monitoring system. Finally, Section 4 delves into a discussion of our results, encompassing an overall discussion of the flexible smart water gauge, the velocity accuracy test, and a thorough error analysis. Finally, this structured approach culminates in the conclusion, providing a summary of the research. Figure 1 shows the prototype of our flexible smart water gauge.

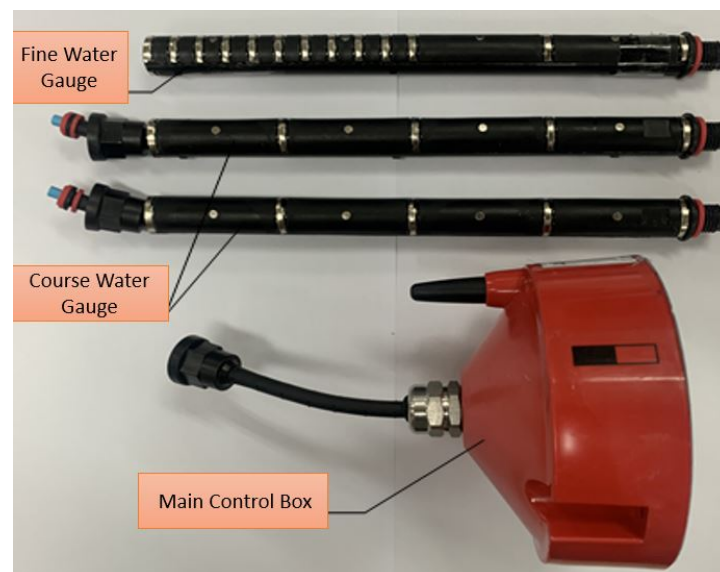


Figure 1. Flexible smart water gauge prototype.

The design inspiration for the flexible smart water gauge sensor was a motion device that uses mechanical and electronic components or intelligent materials to achieve underwater propulsion according to the propulsion mechanism of fish when swimming [30]. The movement of fish has the characteristics of high efficiency, high maneuverability, and low noise [31,32]. Through researching bionic robot fish, we combined measurements of water level, velocity, flow, and flow direction with a multi-joint activity mechanism to design a flexible smart water gauge, as shown in Figure 2 below.



Figure 2. Bionic robot fish to flexible smart water gauge.

2.1. Basic Principles

The smart water gauge is a water measuring instrument suitable for use in urban drainage pipes, urban water accumulation areas, reservoirs, lakes, rivers, and other similar environments. It is easy to install and maintain, comprising four main components: the main control box, connector, ring cable, probe, and adapter board (accessory). The detection electrode (stainless steel conductive ring) is installed on the ring wire ruler according to the corresponding spacing for resolution and is encapsulated in the casing together with the acquisition CPU and the low-power step-down power supply. This setup leaves only the contact part exposed to the casing.

When the control system is powered on or receives a measurement command, the smart water gauge initiates a measurement cycle and transmits the status of the measurement points and water level height data through the serial port. During the measurement process, the acquisition CPU activates the measurement power of electrodes in different areas according to a specific pattern, reads the status of the input interface of the measurement CPU in turn, scans all the detection electrodes in batches in a matter of milliseconds, and calculates the water gauge's measured value using the built-in algorithm model.

The data are then transmitted to the external data acquisition instrument through the data lead, facilitating the calculation of the distance from the water gauge measurement to the water surface. The smart water gauge gathers relevant monitoring data, promptly transmits and stores them in the cloud server, and enables data sharing with designated parties. Generally, the smart water gauge remains in a standby or power-off state to conserve power in the measurement circuit.

Furthermore, the smart water gauge is equipped with a remote switching function to adapt to different weather conditions on dry and rainy days. During dry days, the scanning frequency of the smart water gauge is reduced, with a scanning period of 1–2 min and a reporting communication period of 5–15 min. In the event of emergencies, the scanning frequency is increased to 15 s, ensuring the smart water gauge's service life.

Principles of Collecting Water-Level Data

The flexible smart water gauge positioned at the bottom of the manhole cover operates as a contact-type water gauge. It gathers water depth information using a series of electrodes evenly distributed across the water gauge body. By assessing which electrodes are submerged in water, the water depth can be determined. The elevation of the manhole cover at this particular point is measured using RTK dynamic carrier phase difference technology, enabling the assessment of the water level at that point. This technology finds extensive application in monitoring liquid levels in urban underground pipe networks, urban sewage treatment facilities, rivers, lakes, and other similar projects. The schematic diagram below illustrates the arrangement of the water gauge equipment under the manhole cover.

Figure 3 illustrates that the structure of the flexible water gauge body consists of a single-section measuring structure, which is linked with multiple sections, and these two sections of the water gauge are interconnected by a waterproof plug and socket. As the flexible smart water gauge is composed of multiple cascaded sections, the elastic deformation of the cable can influence the water flow, leading to an impact on the angle of

the single section of the water gauge. Consequently, this can result in a significant error in the detection data of the draft gauge.

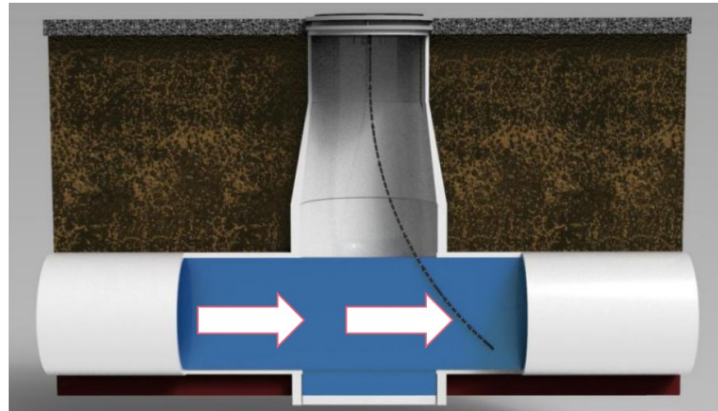


Figure 3. The schematic diagram of equipment installation.

To address this issue, a pitch angle sensor is incorporated into the water gauge. This sensor is responsible for detecting the deflection angle of each section of the water gauge. It then calculates and analyzes the water level of the monitoring point based on the obtained angle of each section of the water gauge. The principle is elucidated in the analysis presented in Figure 4 below.

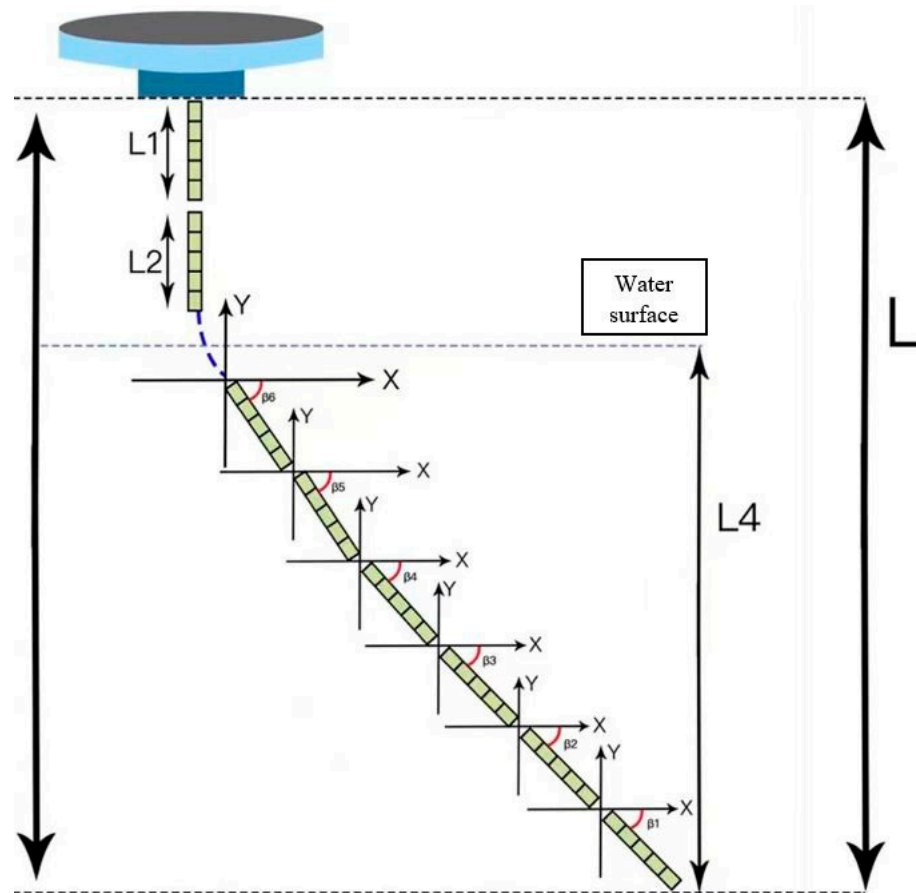


Figure 4. Schematic diagram of water level calculation of manhole cover terminal equipment.

Initially, it is understood that the elevation of the manhole cover node is denoted as L with the unit of measurement being meters (m). The theoretical length of the natural

sag after the cascaded length of the terminal draft is represented as $h1$, while the vertical length of the draft after natural deflection due to water flow is denoted as $h2L2$. The data provided indicate that the dip angles of each section of the water gauge from bottom to top are $\beta_1, \beta_2, \beta_3, \beta_4, \dots, n$. Utilizing RTK technology, it is determined that the length of each section of the water gauge is $L = 0.25$ m, with an additional length denoted as $L1 = 0.3$ m. Assuming that the number of sections of the water gauge is n , the total height of the water gauge in its naturally sagging position can be calculated.

$$h1 = l(n - 1) + l1 \quad (1)$$

Firstly, during the operational use of the water gauge, it bends due to the influence of water flow, and each section is equipped with an attitude sensor that records the inclination of the water gauge. Assuming the inclinations of each section of the draft gauge from bottom to top are $\beta_1, \beta_2, \beta_3, \beta_4, \dots, n$, the total height of the draft gauge under bending conditions is $h2L2$, given by the following equation:

$$\sum_i^{n-1} \sin\beta_i + \sin\beta_n \quad (2)$$

Secondly, during actual operation, the uploaded data are represented as $h3$, which is the theoretically vertical height uploaded, disregarding the bending state of the water gauge. However, the uploaded data do not represent the actual height of the water gauge immersed in the water. Thus, it is necessary to determine the exact height of the flexible smart water gauge in the water by calculating the number of water gauge sections submerged in the water and the inclination of the stored water gauge. Assuming the actual number of water gauge sections immersed in the water is t , the section between the water surface being the $(t + 1)$ section, t is calculated as follows:

$$t = [h3/l] \quad (3)$$

where the function $y = [x]$ denotes the rounding function, which takes the largest integer that does not exceed x as $[x]$. Equation (3) indicates that section $(t + 1)$ is between the water surfaces, the water gauge of section t is fully immersed in the water, and the vertical height $h4L4$ after the natural deflection of the water gauge immersed in the water is determined by section $(t = 1)$. The vertical height of t and the vertical height of the t -saved gauge fully immersed in water are given as follows:

$$L4 = (h3 - t * 1) \sum_i^t 1 * \sin\beta_i \quad (4)$$

Finally, by calculating the vertical height $h2L4$ of the water gauge after natural deflection and the vertical height $h4L4$ of the water gauge immersed in the water, the water gauge's height above the water surface is obtained. Combined with the elevation of the manhole cover node denoted as L , the water level of the flexible smart water gauge is calculated as follows:

$$H_{\text{waterlevel}}(H_{\text{wl}}) = L - L2 + L4 \quad (5)$$

The water level data of the manhole cover node can be acquired by inputting the original data of the manhole cover node into the formula on the server side. Upon obtaining the data from the manhole cover node, the node's water level data are analyzed. If the data indicate that the water level has risen by more than 20 cm within 15 min, an immediate alarm is triggered. Similarly, an alarm is also initiated if the water level exceeds two-thirds of the manhole cover node's elevation. Other data are automatically stored on the server side for historical data queries. The processing of water level data under the manhole cover node is detailed in Table 1 below.

Table 1. Judgment table of water level data processing.

Water Level	Water Level	Handling the Situation
The water level rises over 20 cm within 15 min.	Abnormal	Immediate processing
The water level is greater than 2/3 of node height.	Abnormal	Immediate processing
Another condition.	Normal	Not processing

2.2. The Principle of Flexible Smart Water Gauge Flow Rate Data Acquisition

The specific algorithm for the flexible smart water gauge to measure the flow rate is as follows:

- (1) Use a flow meter to measure the flow velocity at different depths at the same test point in the same water area, and obtain the accurate value $V0i$, which is, respectively, recorded as $V01, V02, \dots, V0n$;
- (2) Use the detection ruler of the flexible smart water gauge to measure the flow velocity at different depths of the same test point in the same water area described in step (1), respectively, obtain the initial value of the angle measured by the angle sensor Ci , and repeat the measurement m times to obtain the average value, the initial angle average value is obtained, and the initial angle average values measured by n angle sensors are recorded as $W01, W02, \dots, W0n$, m is a positive integer $m \geq 3$;
- (3) Convert the Angle $W0i$ into the initial flow rate $V0i$;

$$T * \cos W0i = mg \tag{6}$$

$$T * \sin W0i = P\Delta S \tag{7}$$

$$\Delta S = l * 2r \tag{8}$$

Here, m signifies the weight of each section of the detection ruler, while T denotes the tensile force of each section of the detection ruler. $f = p\Delta S$ represents the impact force of each section of the detection ruler caused by the flowing water, with p being the pressure of the corresponding section of the flowing water at different depths on the ruler, ΔS representing the area of the water-facing surface of each section of the detection ruler, and r indicating the outer diameter of the second insulating shell. Bernoulli's equation for fluids is also utilized, given as follows:

$$p + \rho g h_i + \frac{1}{2} \rho V_{0i}^2 = Q \tag{9}$$

where Q is a constant and ρ is the density of the liquid, the depth corresponding to the i th angle sensor.

$$h_i = l(\cos W01 + \cos W02 + \dots + \cos W0i) \tag{10}$$

It can be obtained from the Formulas (6)–(10)

$$V01 = \sqrt{\frac{2Q}{\rho} - 2gl(\cos W01 + \cos W02 + \dots + \cos W0i) \frac{mg * \tan W0i}{l * r}} \tag{11}$$

- (4) Comparing the $V0i$ in step (3) with the $V0i$ in step 1, we obtain

$$V0i = k_i.V_i + d_i \tag{12}$$

That is the correction coefficient that is obtained, where i is a positive integer $1 \leq i \leq n$, k_i is the first correction coefficient, and d_i is the second correction coefficient. By using a flow meter to measure the flow velocity at different depths of the same test point in

the same water area, an accurate value V_{0i} is obtained; then, we used the detection ruler of a flexible water gauge to measure the flow velocity at different depths of the same test point in the same water area and obtain the angle. The initial value of the angle was measured by the sensor C_i , and then the first correction coefficient and the second correction coefficient d_i were obtained.

- (5) Place the flexible smart water gauge at the point to be detected with the detection water area, so that the 0 scale line of the detection ruler is flush with the horizontal plane;
- (6) Due to the different flow rates of water at different depths h_i , the inclination angles of the flexible water gauges of different sections are different. Each angle sensor measures the inclination angle W_i of the corresponding flexible water gauge and transmits it to the control module. The control module converts the calculation of W_i into the calculated value V_i , and applies the Formula (11) to obtain

$$V_{01} = \sqrt{\frac{2Q}{\rho} - 2gl(\cos W_1 + \cos W_2 + \dots + \cos W_i) \frac{mg * \tan W_{0i}}{l * r}} \quad (13)$$

$$V_i = k_i.V_i + d_i \quad (14)$$

The Formulas (13) and (14), and the corresponding first correction coefficient k_i and second correction coefficient d_i , are stored in the control module to form a calculation model, so it is only necessary to transmit the angle value detected by the angle sensor in real-time to the control module, and then the flow rate of the water flow can be obtained.

2.3. Manhole Cover Terminal Equipment Flow Rate Calibration

Standard Flow Meter

The flow rate calibration experiment of the manhole cover terminal equipment uses the LS1206B propeller flow meter, which is manufactured by Shenzhen Graigar Technology Co., Ltd China, as shown in Figure 5. The LS1206B propeller flow meter is widely used for average tassel measurement in rivers, lakes, reservoirs, and pipelines. It is a commonly used universal testing instrument for hydrological data collection. The main working parts of the LS1206B propeller flow meter include a propeller, tail components, reed switch, support seat, and extendable bracket. When measuring the flow rate of water, the propeller rotates due to the impact of the water flow. The rotation of the propeller drives the rotor to rotate synchronously. The rotation of the rotor causes its magnet to generate an excitation signal for the reed switch, and the detection circuit, therefore, generates an on-off signal. By detecting and recording the number of on-off signals and the on-off times, the average flow rate of the water flow can be calculated.

When the water flow speed is higher than the critical speed, there is a stable linear relationship between the average flow speed at the detection point within a certain period and the rotor of the LS1206B propeller flow meter. Under the premise of ensuring a certain accuracy, the average flow speed satisfies the following relationship:

$$v = a + bn \quad (15)$$

where

v : flow velocity (average flow velocity during the period), m/s;

a : flow meter constant, m/s;

b : propeller hydraulic pitch, m;

n : velocity meter rotor speed, $\frac{1}{s}$.



Figure 5. LS1206B propeller flow meter.

$$n = R/T \quad (16)$$

where;

R : total number of rotors of flow meter;

T : speed measurement duration, s.

To eliminate the influence of water flow on the measurement accuracy, the hydrological inspection specification requires that the general $T \geq 100$ s. It can be obtained from the following Formula (17):

$$v = a + b \frac{N}{T} \quad (17)$$

where

N : the number of signals in the T period.

To determine the values of a and b , please refer to the verification results given in the GB/T21699-2008 [33] (<https://www.gbstandards.org/>, accessed on 1 December 2021) standard for the Verification/Calibration Method of Rotor Flow Meters in Linear Slots", $a = 0.0159$ m/s, $b = 0.1188$ m. Therefore, the determination of the flow rate only needs to measure T and N to calculate the flow rate; the formula is as follows:

$$v = 0.0159 + 0.1188 \frac{N}{T} \quad (18)$$

According to the calculation principle of open channel flow, the flow value is the product of the flow velocity and the cross-sectional area of the measuring point. Therefore, the accuracy verification of the manhole cover terminal water gauge only needs to verify the accuracy of the flow rate.

3. Result

3.1. Water Level Accuracy Experiment

The equipment's overall design requirements entail several crucial considerations. Firstly, the detection range, detection accuracy, and minimum operational range of the water level beneath the manhole cover must be taken into account. Secondly, the size of the detection equipment should align with the installation constraints within the manhole cover. As the water gauge equipment needs to be immersed in water, it should be designed with flexibility and scalability to accommodate the uncertain water levels beneath the manhole cover. In addition, since the manhole cover is consistently exposed to a humid environment,

the testing equipment itself must satisfy waterproof and rust-proof prerequisites. To meet the specifications for application in Nanjing's Jiangning District, terminal monitoring equipment must adhere to the comprehensive design requirements specified in Table 2 below. Consequently, the Flexible Smart Water Gauge (FSWG) was purposefully designed to align with these established standards. The criteria for the Jiangning District were determined by the authorities at the Huadong Testing Center in 2021. This decision followed a meticulous on-site examination of diverse manhole covers and river conditions in the district, complemented by technical consultations with engineering professionals.

Table 2. Overall design requirements for manhole cover terminal monitoring equipment.

Serial Number	Items	Design Index
1	Water level measurement range	0–5000 mm
2	Water level measurement accuracy	10 mm, 50 mm
3	Minimum working range	250 mm
4	Coarse/fine water gauge deflection angle	0~180°
5	Coarse/fine water gauge deflection angle accuracy	±2°
6	Maximum operating temperature	70 °C
7	Minimum operating temperature	–20 °C
8	Waterproof level	IP68 level
9	Length of Water Gauge	It can be extended by cascading

The measurement of water level information mainly detects the depth of the equipment immersed in water and the elevation information of the manhole cover node through the water gauge and deduces the water level data of the manhole cover node. Therefore, the accuracy test for the water level of the equipment is mainly to test whether the length detection of the equipment immersed in water is accurate. The water level accuracy test of the water gauge was tested by using three sets of equipment prototypes with three main control boxes cascaded with three water gauges. The experimental platform shown in Figure 6 was built. The experimental platform comprises metal brackets, test buckets, and terminal equipment. The length of a single section of the water gauge is 250 mm, and the different states of the water gauge are tested.

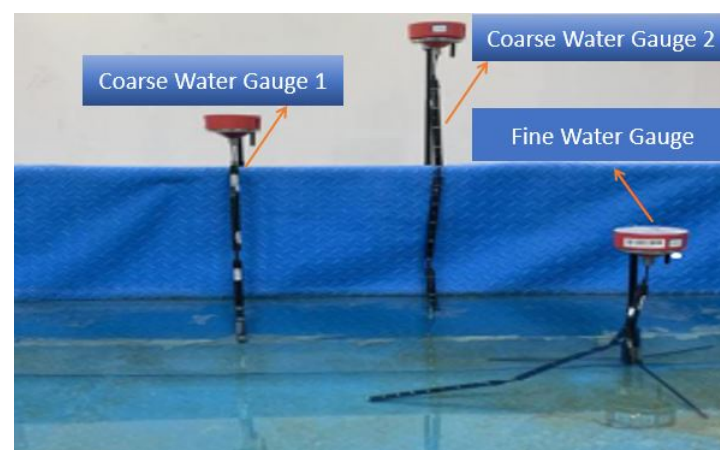


Figure 6. Construction of water level detection environment.

The various states are primarily classified into the following five scenarios:

- (1) The water gauge does not touch the water surface, and the fine water gauge 1 is positioned above the water surface.
- (2) The water level is within the range of the fine water ruler 1, with the submersion depth of fine water ruler 1 falling between 0 and 250 mm.

- (3) The water level is not higher than the fine water gauge 1 but lies between the coarse water gauge 2. The submersion depth of the fine water gauge 1 ranges from 250 mm to 500 mm.
- (4) The water level is not higher than both the fine water gauge 1 and coarse water gauge 2 but falls within the coarse water gauge 1. The submersion depth of the fine water gauge 1 ranges from 500 mm to 750 mm.
- (5) The water surface is below the fine water gauge 1, coarse water gauge 2, and coarse water gauge 1. The submersion depth of the fine water gauge 1 is more than 750 mm. Currently, the water surface exceeds the maximum range of the device, and the water surface height display is set to 750 mm. Three sets of experiments are conducted for each water gauge situation, and the experimental data of the immersion depth of the equipment prototype in the APP is presented in Table 3 below.

Table 3. Experimental data table of five conditions of water scale.

Serial Number	Actual Immersion Depth (mm)	Uploaded Data Size (mm)	Whether it Meets the Accuracy Requirements
1	−35	0	Yes
2	−100	0	Yes
3	−180	0	Yes
4	35	30	Yes
5	100	100	Yes
6	180	150	Yes
7	280	250	Yes
8	330	300	Yes
9	480	450	Yes
10	540	500	Yes
11	610	600	Yes
12	680	650	Yes
13	760	700	Yes
14	800	700	Yes
15	850	700	Yes

Table 3 provides the experimental data collected under five distinct water gauge scenarios, each characterized by specific conditions and submersion depths. These scenarios encompass a comprehensive range of water levels and immersion depths, allowing for a comprehensive evaluation of the flexible smart water gauge sensor's performance across varying conditions. Notably, the data demonstrate that the device consistently meets the accuracy requirements across all the defined water gauge situations, indicating its robust functionality and reliability.

In the first scenario, where the water gauge does not touch the water surface, the device successfully maintains accurate measurements, reflected in the data entries displaying negative immersion depths. Similarly, in scenarios two through five, where the water levels correspond to different ranges within the fine and coarse water gauges, the device consistently exhibits precise measurements, as indicated by the uploaded data sizes aligned with the specific submersion depths.

These results emphasize the device's ability to effectively adapt to diverse water level conditions, ensuring accurate measurements even in challenging situations where the water levels surpass the device's maximum range. The successful outcomes of the three sets of experiments conducted for each water gauge scenario reaffirm the device's reliability and validate its capacity to meet the accuracy requirements across various immersion depth scenarios.

3.2. Verification Experiment of Flexible Smart Water Gauge Flow Rate

The measurement accuracy of the flow velocity of the flexible water gauge is verified by the control group experiment of the standard flow meter and the flexible water gauge of

the manhole cover terminal. The experimental site is the Hydrology and Water Resources Experimental Center of Hohai University. The river channel model consists of a reservoir, a pump room, a backwater gallery, a water tank, and a tailgate. The tank is 55 m long, 3 m wide, and 1.5 m high. The maximum flow through is $0.75 \text{ m}^3/\text{s}$. First, the terminal flexible water gauge and the standard flow meter are fixed on the same bracket and arranged in the backwater corridor as a whole, as shown in Figure 7 below.



Figure 7. Experimental arrangement of terminal flexible water gauge and standard flow meter.

Turn on the switches of the reservoir and pump room to ensure that the water surface is immersed in the terminal water gauge and the standard flow meter. The experimental states of the terminal flexible water gauge and the standard flow meter are shown in Figure 8a,b. After the water flow first passes through the propeller of the LS1206B propeller-type flow meter, the flexible smart water gauge is deflected by the impact force of the water flow and the water flow of each section of the water gauge is recorded. The deflection angle is brought into the flow rate algorithm for calculation. The flow rate data of some flexible smart water gauges and standard flow meters obtained by the experiment are shown in Table 4.



Figure 8. Experimental state of standard flow meter (a) and flexible smart water gauge (b).

Table 4. Comparison of flow rate data between standard flow meter and flexible smart water gauge.

Serial Number	Standard Flow Meter (m/s)	Flexible Smart Water Gauge (m/s)	Error (m/s)
1	0.298	0.282	0.016
2	0.289	0.273	0.016
3	0.312	0.301	0.011
4	0.309	0.280	0.029
5	0.331	0.321	0.012
6	0.333	0.322	0.011
7	0.324	0.312	0.012
8	0.247	0.210	0.037
9	0.259	0.220	0.039
10	0.265	0.252	0.013

Table 4 presents the results of comparing the standard flow meter (SFM) and the flexible smart water gauge (FSWG) for measuring water flow velocity. The measurements were taken in meters per second (m/s), and the third column shows the difference or error between the two instruments. The SFM represents the best measurements obtainable at present, suggesting that the FSWG is sufficiently accurate in most cases, with deviations attributed to issues with the instrument. This is evident in the error column, where most values are positive, indicating that the SFM overestimated velocity compared to the FSWG. However, it is worth noting that the magnitudes of the errors are relatively small, with most values ranging between 0.01 and 0.04 m/s. This suggests that both instruments can provide reasonably accurate measurements of flow velocity. It is also observable that some measurements exhibited a larger discrepancy between the two instruments, such as measurements 4, 8, and 9, which had errors of 0.029, 0.037, and 0.039 m/s, respectively. Hence, the data presented in Table 4 provide insights into the performance and precision of these two measurement systems in terms of flow rates. They serve as a comprehensive source of flow velocity information, allowing for an assessment of the accuracy of the equipment, specifically when comparing the Standard Flow Meter (SFM) and the Flexible Smart Water Gauge (FSWG).

3.3. Implementation of Intelligent Manhole Cover Monitoring System

The manhole cover terminal equipment has undergone verification through the above experiments and meets the requirements for monitoring manhole cover nodes. The following presents the equipment layout for the actual underground pipe network of the Jiangning Campus of Hohai University. Based on the construction diagram of the campus's rainwater and sewage underground pipe network, 38 manhole cover nodes were chosen for the installation of the equipment. The selection spot of manhole cover terminal equipment on the Jiangning Campus of Hohai University is depicted in Figure 9.

The layout of the manhole cover terminal involves three main steps. Firstly, it is necessary to measure the water depth of the installed manhole cover node, primarily using a water level measuring instrument that emits a buzz when it touches the water surface. Subsequently, the water surface data of the manhole cover are read. Figure 9 illustrates the water level measuring instrument in action, measuring the depth of the manhole cover node. Secondly, based on the depth measured by the water level instrument, the appropriate number of manhole cover terminal pools is selected to ensure that a portion of the water gauge is immersed in water. The on-site completion and debugging of the manhole cover terminal equipment are shown in Figure 10.



Figure 9. Actual depth of manhole cover node measured by water level meter.



Figure 10. Manhole cover terminal water gauge after field debugging.

Finally, drill holes on the body of the manhole cover according to the size of the mounting bracket. As vibration is generated when a vehicle passes by, M6 type bolts and nuts are used, and an M6.5 type impact drill is employed. The manhole cover terminal equipment is installed through the bracket, and the installed manhole cover node is depicted in Figure 11.

By repeating the above steps, install and debug the rainwater and sewage manhole cover terminal equipment. After the installation, view the data information of 10 manhole cover terminal water gauges in the APP terminal. Following the outfield layout, some equipment information results are shown in Table 5. At this point, the Hohai University Jiangning Campus manhole cover terminal water gauge equipment field layout is completed.

The “Rainwater” column indicates the amount of rainwater measured at each monitoring point. Rainfall values vary across the monitoring points, ranging from 2 mm (Rain 007) to 25 mm. Water levels range from 2 mm (Rain 007, Rain 010) to 25 mm (Rain 001, Rain 002, Rain 006). Flow velocities vary across the monitoring points, ranging from 0.102 m/s (Rain 007) to 0.521 m/s (Rain 001). All points are labeled as “Normal”, suggesting that there are no abnormal conditions reported at the time of measurement.

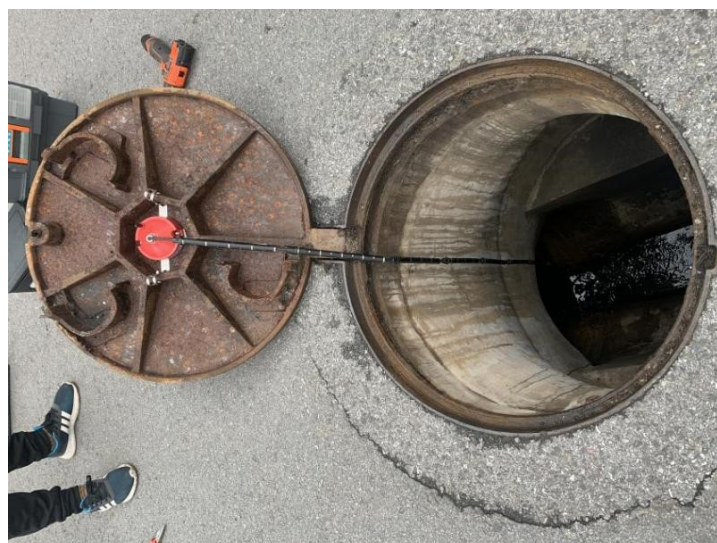


Figure 11. The manhole cover terminal water gauge installed on site.

Table 5. Some equipment information after the outfield layout.

Serial Number	Rainwater	Water Level Information (mm)	Flow Velocity (m/s)	Status	Time
1	Rain 001	25	0.521	Normal	0309–10:00
2	Rain 002	25	0.498	Normal	0309–10:00
3	Rain 003	4	0.112	Normal	0309–10:00
4	Rain 004	3	0.153	Normal	0309–10:00
5	Rain 005	8	0.246	Normal	0309–09:45
6	Rain 006	25	0.486	Normal	0309–10:00
7	Rain 007	2	0.102	Normal	0309–09:45
8	Rain 008	10	0.368	Normal	0309–10:00
9	Rain 0019	6	0.210	Normal	0309–10:00
10	Rain 0010	2	0.104	Normal	0309–10:00

4. Discussion

The integration of smart water gauge technology offers several advantages in monitoring water levels and flow rates for urban drainage and waterlogging prevention. Distinguished by accurate measurement, reliable performance, a compact structure, cost-effectiveness, and easy installation, this technology operates on advanced NB-IOT narrowband Internet of Things technology. Its core encompasses microcomputer technology integrated with intelligent hydrodynamic simulation, facilitating all-weather, maintenance-free, continuous, fixed-point monitoring. The collected data will be efficiently transmitted to a cloud platform, allowing real-time access and early warning.

In terms of power supply, the smart water gauge utilizes a dry battery power supply, allowing for energy conservation through being turned off under normal circumstances. This extends the life of the dry battery, ensuring prolonged usage. The adaptability of the smart water gauge to varying regional conditions is emphasized, requiring specific settings based on local needs and requirements.

4.1. Accuracy Test

The Huadong Testing Center for Hydrological Instruments, under the guidance of the Nanjing Management Department Intelligent Department Care Co., LTD, issued Certificate Number 20210978. The center is located on the seventh Floor, Ren Building, No.7 Yinget Road, Jiangning District, Nanjing. The tested instrument is the Smart Water Gauge with the specification Model AISL1501, manufactured by Nanjing Management Intelligent Technology Co., LTD. The testing utilized a straight-line channel and a flow meter verification

device, both meeting the value traceability standards as per basic environmental experimental conditions and methods of hydrologic instruments. The testing conditions included a mixing ratio of 65.9%, water temperature at 8.0 °C, room temperature at 13.5 °C, and air pressure of 101.11 kPa. The assessment was conducted on 23 April 2021.

4.1.1. Velocity Accuracy Test

The results from the velocity measurement record conducted by the Huadong Testing Center for Hydrological Instruments provide a comprehensive assessment of the Smart Water Gauge’s performance. The table presents the measured values across different standard velocities, with corresponding average values and errors calculated, as shown in Table 6 below.

Table 6. Velocity accuracy test record.

Serial Number	Standard Value (m/s)	Measured Value (m/s)	Average Value (m/s)	Error (m/s)				
1	0.0500	0.0305	0.0515	0.0515	0.0535	0.0435	0.0461	0.0039
2	0.1000	0.0965	0.0915	0.0907	0.0952	0.1091	0.0966	0.0034
3	0.2000	0.2158	0.2251	0.1978	0.1925	0.1895	0.2041	0.0041
4	0.5000	0.5346	0.5103	0.4895	0.4917	0.5037	0.5059	0.0059
5	1.0000	1.0710	1.0958	0.9726	0.9573	1.0214	1.0236	0.0236
6	2.0000	2.0345	2.0176	1.9875	1.9936	2.0287	2.0123	0.0123
7	2.5000	2.4987	2.4865	2.5170	2.5213	2.4985	2.5044	0.004

Upon analysis, it is evident that the measured values closely align with the standard values for each velocity category. The average values consistently demonstrate a high degree of accuracy, showcasing the reliability of the Smart Water Gauge in capturing velocity measurements. The calculated errors for each detection point, ranging from 0.0039 to 0.0236 m/s, are well within the acceptable range. Furthermore, the overall assessment, as indicated by the root mean square error of 0.011 m/s, affirms the equipment’s precision. The error being less than 5% + 0.02 m/s across all detection points underscores the consistent and reliable performance of the Smart Water Gauge. This level of accuracy is crucial for hydrological applications where precise velocity measurements are paramount.

4.1.2. Error Analysis

An error analysis chart between the indicator flow rate and measured flow rate of a smart water gauge is shown in Figure 12 below. Compared with the measured average flow rate, the correlation coefficient is 97.1%. The relative error of less than 5% accounts for 92%, and the relative error of less than 6% accounts for 100%. The root mean square (RMS) error is 2.5 cm/s, and the RMS velocity relative error is 2.3%. The overall error is less than 5% + 0.02 m/s.

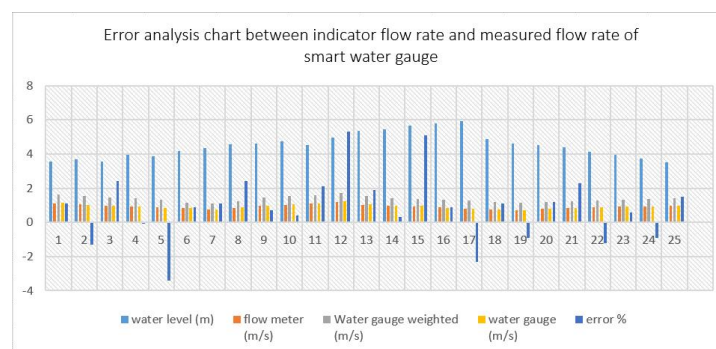


Figure 12. Error analysis chart between indicator flow rate and measured flow rate of smart water gauge.

The smart water gauge river flow calculation and measured flow rate analysis is shown in Figure 13; compared with the calculated flow rate of the Smart Water Gauge and the measured flow rate in the laboratory, the correlation coefficient is 96.5%. The relative error of less than 5% accounts for 76%, the relative error of less than 8% accounts for 92%, and the relative error of less than 10% accounts for 100%. The root mean square relative error is 3.9%.

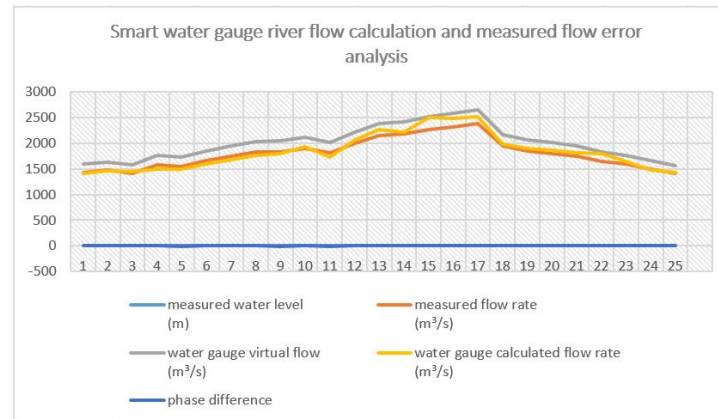


Figure 13. Smart water gauge river flow calculation and measured flow rate analysis.

4.1.3. Limitations

Despite its strengths, challenges exist, particularly when the wellbore is full of water or contains numerous impurities. In such conditions, water gauge monitoring may become chaotic, impacting accuracy and efficiency, and rendering the data potentially invalid. As the technology collects more data and continued usage, there are plans for more improvements to address the identified issues.

5. Conclusions

The development and assessment of the flexible smart water gauge represent a significant step forward in the realm of water level monitoring technology. This innovative device, drawing inspiration from the movements of underwater robots previously published from our lab in a robotics journal, combines mechanical and electronic components to ensure precise and adaptable measurements of water parameters. The experiments conducted to evaluate its accuracy underscore its ability to meet the requirements, establishing its reliability in real-world applications.

The immersion data confirm the device's consistent accuracy across all water gauge scenarios, showcasing its reliability even in challenging conditions. Regardless of whether the gauge is not in contact with the water surface or faces water levels beyond its maximum range, the sensor maintains precision. The device consistently delivers accurate measurements across fine and coarse water gauges, validated by aligned data sizes and specific submersion depths. The successful outcomes of the experiments validate the device's reliability, emphasizing its adaptive capabilities and capacity to meet accuracy requirements across varied immersion depths. The comparative analysis with the standard flow meter (SFM) highlighted the flexible water gauge's ability to provide accurate measurements, emphasizing its efficiency and potential for further use. The identified variations in measurement discrepancies underscore the importance of accounting for specific environmental conditions and factors, emphasizing the need for comprehensive calibration and an understanding of contextual influences.

The implementation of the intelligent manhole cover monitoring system at Hohai University's Jiangning Campus demonstrates successful verification and meets the requirements for monitoring manhole cover nodes. A total of 38 manhole cover nodes were strategically chosen based on the campus's rainwater and sewage underground pipe

network. The three-step process, involving water depth measurement using a level instrument, the selection of appropriate manhole cover terminals, and the installation through bracketed drilling, ensure the effective deployment of the monitoring equipment.

The collected data from the rainwater and sewage manhole cover terminal equipment further validate the system's functionality. The varied measurements, including rainwater amount, water level, and flow velocity, demonstrate the adaptability and precision of the monitoring system across different scenarios. Notably, all monitored points report a "Normal" status, indicating the system's reliability in providing real-time information without abnormalities.

Finally, the Huadong Testing Center's confirmation results affirm the flexible smart water gauge's capability to measure velocity, meeting or exceeding the required standards accurately. The minimal errors and adherence to specified tolerances validate the reliability of the equipment, making it a valuable tool for hydrological monitoring and instrumentation.

Looking ahead, the continued advancement of water gauge technology should prioritize refining design elements to accommodate diverse environmental variations and improve measurement precision. Additionally, exploring advanced calibration techniques and signal processing algorithms holds promise for further enhancing the accuracy of water gauge systems, facilitating the more reliable and precise monitoring of water levels and flow velocities. Ultimately, the progress made in this field promises significant contributions to the sustainable management and conservation of water resources, addressing crucial environmental and societal needs.

Author Contributions: Conceptualization, S.W.S.; methodology, S.W.S.; resources, S.W.S. and B.L.; writing—original draft preparation, S.W.S.; writing—review and editing, S.W.S. and B.S.A.; supervision, B.L. All authors have read and agreed to the published version of the manuscript.

Funding: This research received no external funding.

Institutional Review Board Statement: Not applicable.

Informed Consent Statement: Not applicable.

Data Availability Statement: The data presented in this study are available in the article.

Acknowledgments: We are grateful to the Hohai University Experimental sites, who provided the main data set for the study. We also thank the advisors for their valuable support and comments.

Conflicts of Interest: The authors declare no conflicts of interest.

References

1. Zhang, Z.; Zhou, Y.; Liu, H.; Gao, H. In-situ water level measurement using NIR-imaging video camera. *Flow Meas. Instrum.* **2019**, *67*, 95–106. [[CrossRef](#)]
2. Lee, H.K.; Choo, J.; Shin, G.; Kim, S.M. On-site water level measurement method based on wavelength division multiplexing for harsh environments in nuclear power plants. *Nucl. Eng. Technol.* **2020**, *52*, 2847–2851. [[CrossRef](#)]
3. Huang, Q.; Long, D.; Du, M.; Zeng, C.; Li, X.; Hou, A.; Hong, Y. An improved approach to monitoring Brahmaputra River water levels using retracked altimetry data. *Remote Sens. Environ.* **2018**, *211*, 112–128. [[CrossRef](#)]
4. de Vitry, M.M.; Leitão, J.P. The potential of proxy water level measurements for calibrating urban pluvial flood models. *Water Res.* **2020**, *175*, 115669. [[CrossRef](#)]
5. Schelfaut, K.; Pannemans, B.; Van der Craats, I.; Krywkow, J.; Mysiak, J.; Cools, J. Bringing flood resilience into practice: The FREEMAN project. *Environ. Sci. Policy* **2011**, *14*, 825–833. [[CrossRef](#)]
6. Mu, D.; Luo, P.; Lyu, J.; Zhou, M.; Huo, A.; Duan, W.; Nover, D.; He, B.; Zhao, X. Impact of temporal rainfall patterns on flash floods in Hue City, Vietnam. *J. Flood Risk Manag.* **2021**, *14*, 12668. [[CrossRef](#)]
7. Luo, P.; Mu, D.; Xue, H.; Ngo-Duc, T.; Dang-Dinh, K.; Takara, K.; Nover, D.; Schladow, G. Flood inundation assessment for the Hanoi Central Area, Vietnam under historical and extreme rainfall conditions. *Sci. Rep.* **2018**, *8*, 12623. [[CrossRef](#)]
8. Lin, T.; Liu, X.; Song, J.; Zhang, G.; Jia, Y.; Tu, Z.; Zheng, Z.; Liu, C. Urban waterlogging risk assessment based on internet open data: A case study in China. *Habitat Int.* **2018**, *71*, 88–96. [[CrossRef](#)]
9. Sun, S.; Zhai, J.; Li, Y.; Huang, D.; Wang, G. Urban waterlogging risk assessment in well-developed region of Eastern China. *Phys. Chem. Earth* **2018**, *115*, 102824. [[CrossRef](#)]

10. Hu, S.L.; Han, C.F.; Meng, L.P. A scenario planning approach for propositioning rescue centers for urban waterlog disasters. *Comput. Ind. Eng.* **2015**, *87*, 425–435. [[CrossRef](#)]
11. Tang, X.; Hong, H.; Shu, Y.; Tang, H.; Li, J.; Liu, W. Urban waterlogging susceptibility assessment based on a PSO-SVM method using a novel repeatedly random sampling idea to select negative samples. *J. Hydrol.* **2019**, *576*, 583–595. [[CrossRef](#)]
12. Xu, Q.; Chen, P. Comprehensive planning of drainage and waterlogging prevention layout based on urban double repair concept. *Desalin. Water Treat.* **2022**, *268*, 285–295. [[CrossRef](#)]
13. Ning, Y.F.; Dong, W.Y.; Lin, L.S.; Zhang, Q. Analyzing the causes of urban waterlogging and sponge city technology in China. In *IOP Conference Series: Earth and Environmental Science*; IOP Publishing: West Philadelphia, PA, USA, 2017; Volume 59, p. 012047.
14. Wu, J.; Zhang, D.; Chen, Y.; Zhao, Y. A coupled multi-model framework for waterlogging projection: Towards achieving sustainable development goal 11.5. *Urban Clim.* **2022**, *46*, 101305. [[CrossRef](#)]
15. Su, M.; Zheng, Y.; Hao, Y.; Chen, Q.; Chen, S.; Chen, Z.; Xie, H. The influence of landscape pattern on the risk of urban water-logging and flood disaster. *Ecol. Indic.* **2018**, *92*, 133–140. [[CrossRef](#)]
16. Yin, Z.E.; Yin, J.; Xu, S.; Wen, J. Community-based scenario modelling and disaster risk assessment of urban rainstorm waterlogging. *J. Geogr. Sci.* **2011**, *21*, 274–284. [[CrossRef](#)]
17. Colombo, A.F.; Karney, B.W. Evaluation of the long-term energy costs of leaks in buried pipeline systems. In *Underground Infrastructure Research*; CRC Press: Boca Raton, FL, USA, 2020; pp. 197–201.
18. Martini, A.; Troncossi, M.; Rivola, A. Automatic leak detection in buried plastic pipes of water supply networks by means of vibration measurements. *Shock Vib.* **2015**, *2015*, 165304. [[CrossRef](#)]
19. Rockwell, D. The influence of groundwater on surfaceflow erosion processes during a rainstorm. *Earth Surf. Process. Landf.* **2002**, *27*, 495–514. [[CrossRef](#)]
20. Tan, F.; Tan, W.; Yan, F.; Qi, X.; Li, Q.; Hong, Z. Model Test Analysis of Subsurface Cavity and Ground Collapse Due to Broken Pipe Leakage. *Appl. Sci.* **2022**, *12*, 13017. [[CrossRef](#)]
21. Chen, X.; Chen, W.; Zhao, L.; Chen, Y. Influence of Buried Pipeline Leakage on the Development of Cavities in the Subgrade. *Buildings* **2023**, *13*, 1848. [[CrossRef](#)]
22. Grieves, M.; Vickers, J. Digital twin: Mitigating unpredictable, undesirable emergent behavior in complex systems. In *Transdisciplinary Perspectives on Complex Systems: New Findings and Approaches*; Springer: Cham, Switzerland, 2017; pp. 85–113.
23. Xia, H.; Liu, Z.; Efremochkina, M.; Liu, X.; Lin, C. Study on city digital twin technologies for sustainable smart city design: A review and bibliometric analysis of geographic information system and building information modeling integration. *Sustain. Cities Soc.* **2022**, *84*, 104009. [[CrossRef](#)]
24. Masasi, B.; Frazier, R.S.; Taghvaeian, S. *Review and Operational Guidelines for Portable Ultrasonic Flowmeters*; Oklahoma Cooperative Extension Service: Stillwater, OK, USA, 2017.
25. Eren, H. Behaviour of ultrasonic wavefront in multi-phase liquid flow measurements in dosed pipes. In *Quality Measurement: The Indispensable Bridge between Theory and Reality (No Measurements? No Science! Joint Conference-1996, Proceedings of the IEEE Instrumentation and Measurement Technology Conference and IMEKO Tec, Brussels, Belgium, 4–6 June 1996*; IEEE: Piscataway, NJ, USA, 1996; Volume 1, pp. 663–666.
26. Baker, R.C. Turbine and related flowmeters: I. industrial practice. *Flow Meas. Instrum.* **1991**, *2*, 147–161. [[CrossRef](#)]
27. Baker, R.C. *Flow Measurement Handbook: Industrial Designs, Operating Principles, Performance, and Applications*; Cambridge University Press: Cambridge, UK, 2016; pp. 508–510.
28. Chanson, H.; Aoki, S.I.; Maruyama, M. Unsteady air bubble entrainment and detrainment at a plunging breaker: Dominant time scales and similarity of water level variations. *Coast. Eng.* **2002**, *46*, 139–157. [[CrossRef](#)]
29. Sadatomi, M.; Kawahara, A.; Matsuura, H.; Shikatani, S. Micro-bubble generation rate and bubble dissolution rate into water by a simple multi-fluid mixer with orifice and porous tube. *Exp. Therm. Fluid Sci.* **2012**, *41*, 23–30. [[CrossRef](#)]
30. Lou, B.; Ni, Y.; Mao, M.; Wang, P.; Cong, Y. Optimization of the kinematic model for biomimetic robotic fish with rigid headshaking mitigation. *Robotics* **2017**, *6*, 30. [[CrossRef](#)]
31. Cai, Y.; Bi, S.; Zheng, L. Design optimization of a bionic fish with multi-joint fin rays. *Adv. Robot.* **2012**, *26*, 177–196. [[CrossRef](#)]
32. Yan, Z.; Yang, H.; Zhang, W.; Lin, F.; Gong, Q.; Zhang, Y. Bionic fish tail design and trajectory tracking control. *Ocean Eng.* **2022**, *257*, 111659. [[CrossRef](#)]
33. Verification/Calibration Method of Rotating-Element Current Meters in Straight Open Tank. *GB/T21699-2008*; China National Standardization Administration Committee: Beijing, China, 2008.

Disclaimer/Publisher’s Note: The statements, opinions and data contained in all publications are solely those of the individual author(s) and contributor(s) and not of MDPI and/or the editor(s). MDPI and/or the editor(s) disclaim responsibility for any injury to people or property resulting from any ideas, methods, instructions or products referred to in the content.